DOE-CORNELL-0011643

New Methods to Produce and Extend the Spectral Range of Photocathodes for Large Area Photodetectors with mm scale Space Resolution

Final Technical Report

Period covered: May 2014 – March 2019

June 2019

Luca Cultrera and Ivan Bazarov
Cornell University, CLASSE
Ithaca, NY

PREPARED FOR THE U.S. DEPARTMENT OF ENERGY
UNDER CONTRACT NO. DE-SC0011643

Disclaimer

This report was prepared as an account of work sponsored by an agency of the United States Government. Neither the United States Government nor any agency thereof, nor any of their employees, nor any of their contractors, subcontractors or their employees, makes any warranty, express or implied, or assumes any legal liability or responsibility for the accuracy, completeness, or any third party's use or the results of such use of any information, apparatus, product, or process disclosed, or represents that its use would not infringe privately owned rights. Reference herein to any specific commercial product, process, or service by trade name, trademark, manufacturer, or otherwise, does not necessarily constitute or imply its endorsement, recommendation, or favoring by the United States Government or any agency thereof or its contractors or subcontractors. The views and opinions of authors expressed herein do not necessarily state or reflect those of the United States Government or any agency thereof.

Abstract

Cornell group has developed recipes to grow photocathodes belonging to the alkali antimonide family using evaporation from elemental sources with and without line of sight between the sources and the glass substrate. Photocathodes were characterized in terms of their quantum efficiency in the spectral range covering the visible and the near infrared part of the spectrum. Two different approaches have been used to demonstrate the growth of high quantum efficiency photocathodes: the first approach makes use of elemental antimony and alkali metals loaded into ceramic crucibles hosted into effusion cells like the one used in molecular beam epitaxy reactors; whereas in the second approach the antimony film is evaporated onto the transparent substrate using effusion cells and then transferred into a different reaction chamber where exposure to the alkali metals coming from an elemental source lacking the line of sight to the substrate is used to produce the photocathode material.

The research conducted opens the exploration of alternative methods for the synthesis of photocathodes specifically designed to be implemented over large areas maximizing the production throughput and lowering the cost. It particular, this research can benefit future HEP programs by providing new methods that can be adopted to produce photon detectors for future experiments.

1. Introduction

Large area picosecond photodetectors (LAPPD™) have been identified as an enabling detector technology for a wide set of high energy physics (HEP) experiments. Their applications include precision time-of-flight systems in hadron colliders to isolate the region of the primary Z vertex, large water Cherenkov detectors, pre-shower calorimeters for rare kaon decay experiments, and barium fluorescence tagging for neutrinoless double-beta decay experiments [1]. Non-HEP uses of this detector would include medical imaging applications such as time-of-flight positron emission tomography (PET) [2].

The LAPPD Collaboration [3] was formed in June of 2009 to design and provide proof-of-principle of a photodetector with unique properties: large-area, capable of systems of many square-meters, sub-mm spatial resolution, time resolution measured in picoseconds, and competitive in cost per performance with conventional photomultiplier systems. The R&D phase of the project and the Collaboration ended in Dec. 2012 [4] with a transition to commercialization of the LAPPD™ [5] via a 3M$ DOE Technology Transfer Opportunity (TTO) awarded to Incom Inc., the company that manufactures the glass capillary tubes used in the MCPs. LAPPD's have been demonstrated to have gains greater than 10^7, sub-millimeter space resolution for large pulses and several-mm resolution for single photons, time resolutions of 5 ps for large pulses and 50 ps for single photons, high-charge extraction stability against ion feedback, and good uniformity [6-9]. However, the goal of economical production remains yet to be demonstrated; due to the end of the Collaboration only two trials of sealing a complete detector were possible, and while both produced a working tube inside the vacuum production facility, in both cases the seal between the body and the window containing the photocathode (the 'top-seal') leaked when the facility was brought up to atmospheric pressure [10]. Still, the fundamental R&D of making 20-cm square micro-channel glass substrates with 80 million pores, employing Atomic Layer Deposition to produce both a resistive layer and a high-gain secondary emission layer, and the development of low-power inexpensive electronics systems capable of handling many hundreds of channels of sub-10-ps-resolution electronics have all been done [11]. In addition, working top seals have been demonstrated at both Space Sciences Laboratory and the University of Chicago.

The remaining challenge is manufacturability, for which the formation of the photocathode is the key step since its manufacture during assembly determines the level of vacuum and the temperature cycle. The Incom commercialization program [12], a collaborative effort with Space Sciences Laboratory (SSL/UC Berkeley), the University of Chicago, and Argonne Energy Sciences and HEP Divisions, is based on the SSL process, with a much smaller vacuum vessel but the same photocathode and sealing processes (the 'mini-SSL' facility). This is a scalable process for volume production, but it relies on the technically demanding 'vacuum-transfer' of the window after photocathode deposition and subsequent sealing.

In contrast, the conventional batch production of photomultipliers uses the glass envelope of the PMT as the vacuum vessel, with the photocathode made 'in-situ' inside the body. UHV is provided by a high-temperature vacuum bake-out that both cleans the inside and activates an internal NEG getter (adsorption pump). The PMT is typically connected to a low-vacuum system through a glass 'tubulation' at the base of the tube. The tubulation is connected to the vacuum through a simple O-ring gland; after processing the tubulation is flame-sealed by hand. PMT's are made in large batches this way, and although the capabilities of the LAPPD^{TM} cannot be matched by a PMT, the price per tube represents the competition for many large-scale applications such as cryo- or liquid-based neutrino detectors and medical imaging.

Affordable photomultipliers with mm-level spatial resolution and time resolutions in the 10-ps range would be transformational in a number of fields, including rare kaon-decay experiments, low-energy neutrino experiments, collider experiments, neutron detection for national security and reactor monitoring, and x-ray diffraction measurements at light sources. At present, such photodetectors can be made with either micro-channel-plate-based or multi-dynode amplification stages, but they are expensive due to being constructed by vacuum-transfer photocathode synthesis, and consequently not widely used. Within the scope of this award we have studied new methods of photocathode deposition that allow large MCP-based and multi-dynode phototubes to be made without the expensive and time-consuming step of vacuum transfer.

Demonstrating scalable ways of synthesizing large area high quantum efficiency photocathode layers for LAPPD's will open the door for projects requiring large quantities of these devices. In addition, we proposed to extend the usability of LAPPD's by increasing the spectral range of their sensitivity to the near IR photon detection range through the incorporation of Rb_2CsSb and p-n Na_2KSb/Cs_3Sb photocathodes. Among other uses, the potential of using photodetectors with mm-spatial and 10-ps time resolution to separate Cherenkov and scintillation light in large-volume detectors exploits the different spectral shapes of the two sources [13-14].

2. The photocathode growth chamber

During the growth of alkali antimonide photocathodes, the Sb is commonly provided from high purity metallic beads via thermal evaporation. Alkali metal vapors can be obtained using different sources, including alkali metal chromates dispenser [15], bismuth based alloys [16-18], alkali azides [19-20], and by evaporation of pure alkali metals [21]. The use of alkali chromates is advantageous because of their stability with respect to the exposure to open air and their compatibility with UHV environment, whereas alkali azides are also stable in open air, but they release large quantities of nitrogen gas upon decomposition that must be pumped away from the vacuum chamber. Bismuth based alloys and pure alkali metals are extremely reactive and their handling must occur in a glove box in the presence of an inert gas. Because of the drawbacks imposed by the handling of pure metals, only a handful of experiments have been performed to study the growth of alkali antimonide using pure alkalis as precursors demonstrating that

photocathodes with QE comparable to the one reported for commercial devices can be achieved [22-24].

In order to explore the use of effusion cells loaded with pure metals in a geometrical configuration similar to the one adopted in molecular beam reactors for the growth of alkali antimonide based photocathode a new growth chamber was built. We will detail the growth chamber that has been designed and built for this purpose. The design was chosen to be similar to that of the commercial molecular beam epitaxy reactors so that a simple scaling of the chamber should allow growth over larger area substrates suitable for present experiments like the large area photodetectors proposed by the LAPPD^{TM} collaboration [12].

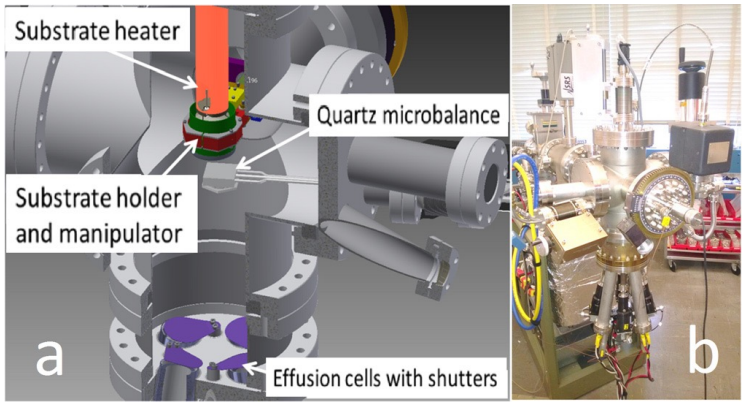

Figure 1 Three-dimensional model (a) and a picture (b) of the UHV growth chamber with effusion cells for evaporation of pure metals.

The experimental setup for the growth of alkali antimonides family photocathodes consists of an UHV vacuum chamber as shown in Fig. 1. It is kept under vacuum by means of a 500 l/s ion pump. The alkali sources assembly is based on an 8 in. diameter ConFlat flange hosting four effusion cells (Varian Mod. 981-4134), each one equipped with its own pneumatically operated shutter. Because of the low melting point of alkali metals, the effusion cells have to be arranged so that the pyrolytic boron nitride (PBN) crucibles sit in an almost vertical position in order to prevent the spill of liquefied alkali metals into the chamber. The angle between the axis of the chamber and the axis of each furnace was chosen to be about 12 degrees. With this geometrical configuration and the 5 degrees of tapering angle characteristic of the PBN crucibles, the system provides a uniform overlap of the molecular fluxes within a 3 in. diameter circular area at about 20 cm distance from the top of the effusion cells.

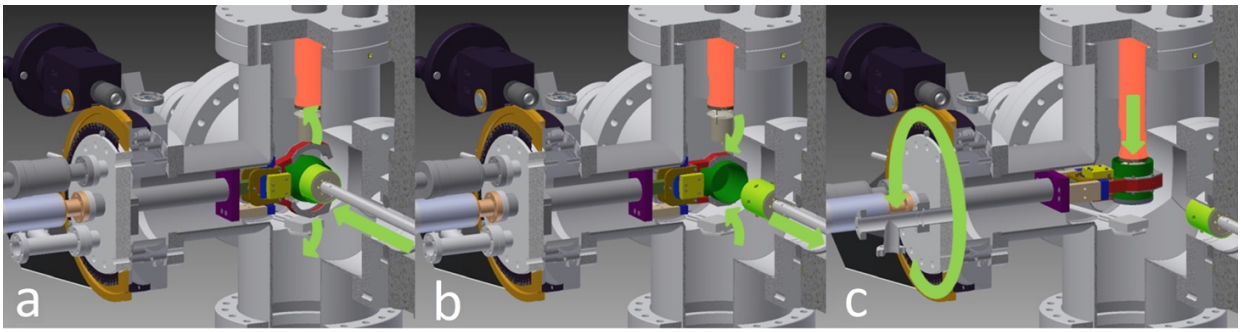

Figure 2 Manipulator and rotary platform operation, which allows the substrate holder to be loaded (a), released (b), and rotated (c) to face the effusion cells hosted in the bottom flange. A resistive heater element is inserted from the top (shown on the right).

In order to ensure compatibility with our other existing experimental vacuum chambers and with the Cornell high voltage DC guns [25,26], a special substrate holder manipulator has been

designed (Fig. 2). This manipulator is hosted by a differentially pumped rotatory platform so that a 90° rotation around the axis can be performed. This rotation gets the substrate holder from the loading/unloading position to the growth position, where the substrate must face the molecular fluxes generated by the effusion cells.

A resistive heater element is inserted from the top flange into the substrate holder and irradiation is used to heat the substrate up to about 600 °C. Two K type thermocouples are connected to the manipulator, and their reading is calibrated to monitor the substrate temperature.

The holder includes several ceramic insulators providing electrical insulation from the UHV chamber so that the substrate can be negatively biased to measure the photocurrent generated from the photocathode materials. In order to minimize the contribution to the photocurrent from stray light getting into the chamber, the light of laser diodes is modulated with a mechanical chopper, and the relative photocurrent is measured using a lock-in amplifier. The QE deduced from the measured photocurrent represents the main signal used as feedback during the synthesis of alkali antimonides photosensitive materials.

A water-cooled quartz crystal microbalance monitors the fluxes from the effusion cells. The microbalance is connected to a linear UHV translator allowing the crystal sensor to be moved just below the substrate surface or at about 2 in. distance from the center of the substrate. Measuring the ratio of the molecular fluxes between the two positions, when the cell is evaporating at a constant temperature, allows deter- mining the tooling factor for each furnace. The tooling factor is then used to scale the quartz microbalance reading during the growth of photocathodes when the crystal sensor is moved away from the substrate.

Because of the high vapor pressure of alkali metals even at room temperature, a bake out of the growth chamber can- not be performed once the effusion cells have been loaded with alkali metals. For this reason, the chamber is baked before loading the metals into each crucible, and the effusion cells and crucibles are degassed by raising their temperature up to 400°C. After the bake, the chamber is vented with a high purity argon gas. A glove box has been designed and built, which allows the refill of the crucible with pure metals under inert gases. The box is made of transparent plastic material to allow seeing the insides from all directions to facilitate the handling of crucibles and alkali ampoules (Fig. 3).

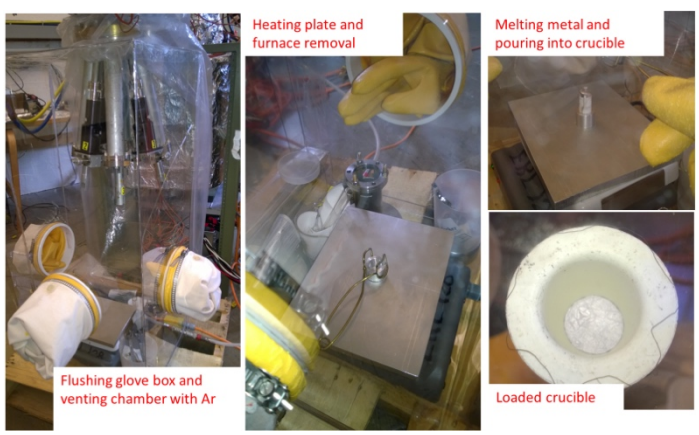

Figure 3 The glove box used refill the crucibles with pure alkali metals in a controlled Ar atmosphere. Picture from different steps of the crucible refill are here reported.

Once the growth chamber has been baked and the crucible thoroughly degassed under vacuum, the glove box is connected to the growth chamber that hosts the furnaces and the whole system is vented with dry argon. The furnaces are then removed and a heating plate sitting in the glove box is warmed up. The ampoules containing the alkali metals are opened and the metal is left in

contact with the heating plate until it melts. At this point, the liquid alkali is poured into the ceramic crucibles and the furnace is reconnected to the growth chamber. Once all the cells have been refilled and reconnected, the growth chamber is pumped down to UHV. Effusion cells' crucibles are filled with 5 g of Cs, K, Na, Rb or Sb each. After 24 h of pumping, the vacuum level reached a typical level of few 10^{-8} Torr. Refer to Fig. 4 for the mass spectrum as measured with a residual gas analyzer (SRS RGA-200).

The mass spectrum in Fig. 4 is hydrogen dominated along with water vapors in the low 10^{-10} Torr range. It is important for water vapors to be kept as low as possible to avoid poisoning of the photocathode during and after the growth. Assuming a sticking coefficient equal to one, the time for the formation of a single monolayer of water vapor is estimated to be about 3 h. From the mass spectrum, we can also see that Cs vapors are already detected even with the effusion cell kept at room temperature; the measured partial pressure for singly ionized Cs ions is in the 10^{-11} Torr range (which is equivalent to a time span of few hours for the formation of a single monolayer over the photocathode surface).

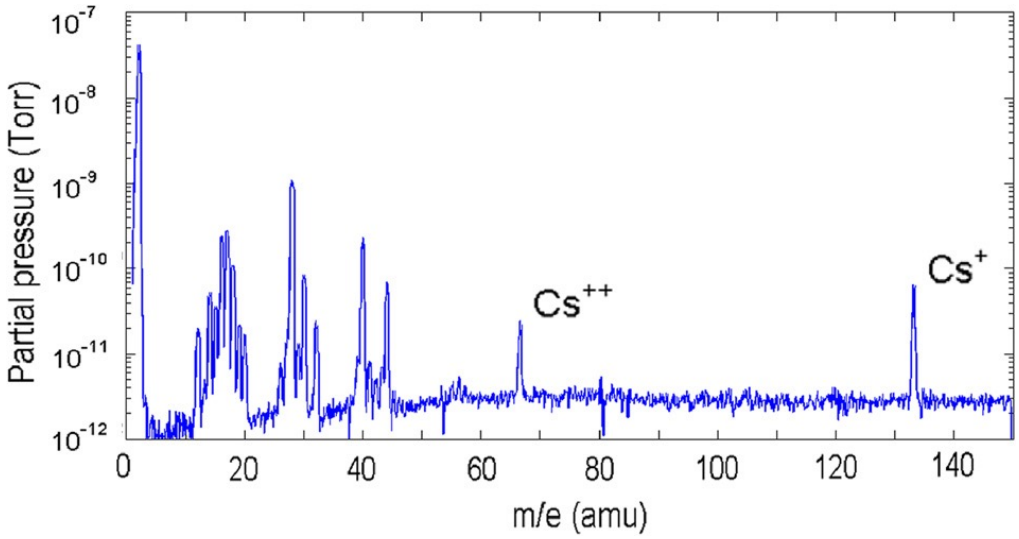

Figure 4 RGA mass spectrum of the growth chamber: peaks of Cs single and doubled ionized are labeled.

3. The "in-situ" growth system

Furthermore, in addition to the conventional growth, we proposed to test the new idea of synthesizing the alkali antimonides photocathodes by chemical reaction with a pre-deposited Sb layer and alkali metal vapors generated with sources not having a direct line of sight to the substrate surface. This second set of experiments, which has never been attempted before, was intended to seek a viable path to produce a photocathode in a sealed planar photodetector like the proposed LAPPD^{TM}, where the glass window is coated with a pre-deposited Sb thin film that has been temporarily exposed to ambient air or controlled atmosphere to perform the detector tile sealing.

In large area planar LAPPD™-like device, a thin gap on the order of a few mm exists between different elements comprised into the stack. These geometrical constraints make it impossible to achieve a uniform exposure of Sb layer to alkali metal vapors with a conventional source that generates a molecular beam flux. To perform the uniform Sb exposure to alkali vapors we propose to transport alkali metals by means of an inert carrier gas to the pre-deposited Sb surface as illustrated in Fig. 5.

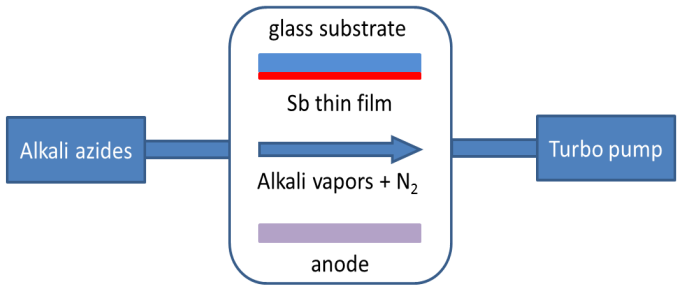

Figure 5. Schematics representation of the process envisaged to introduce alkali metal vapors into the planar detector structure to react with the pre-deposited Sb layer to produce the photocathode material.

To perform this task, we intended to take advantage of the unique property of alkali azides, which, once heated under vacuum close to their melting point (about 300 °C), dissociate releasing pure nitrogen gas and alkali metals. Our previous experimental results demonstrated that alkali azides are a viable alternative for generating alkali metals vapors with the purity needed to perform the growth of high efficiency alkali antimonides photocathodes and that as expected the nitrogen gas released in the decomposition does not affect the photocathode properties [20]. Therefore, we believe that a pre-deposited Sb layer on a glass substrate placed in a small vacuum vessel, in which a suitable pressure gradient is established by pumping through one port while a mixture of alkali metal vapors and nitrogen generated by alkali azide thermal decomposition is entering through another port, can be made to react with the alkali metal vapors flowing into a narrow gap to form a high quality photosensitive material. Cs and Rb, being the most volatile elements, appear to be the most promising elements to perform the initial tests, but K and Na will also be used for this purpose. Another advantage in using azides lies in the intrinsic stability of these chemicals that greatly simplifies their handling. On the other hand, the thermal decomposition of the azide molecules does not allow fine-tuning the ratios between the alkali metal vapors and the nitrogen fluxes. However, high quality nitrogen gas can be easily injected inside the furnace where the azide is being decomposed. An adequate temperature gradient should also be established across the vacuum vessel to favor the deposition of the alkali metal over the Sb layer on the glass window.

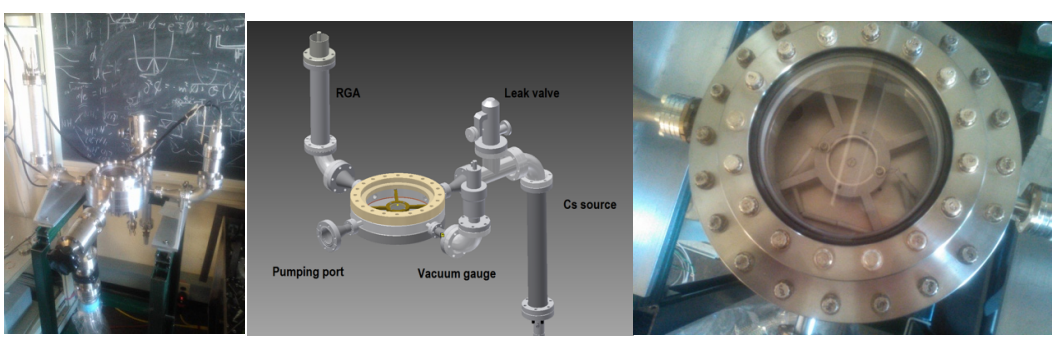

Figure 6. The 3d model of the chamber designed to perform Sb activation in a configuration similar to the LAPPD™ shown on the central picture. On the left the chamber as assembled and on the right a detail of the reaction chamber and sample holder.

In order to perform this set of experiments a new chamber needed to be designed and built. A 3D model of the adopted designed and pictures of the chamber are reported in Fig. 6.

Unfortunately, once the chamber was already built, we could not find any supplier for the Cesium Azide salt with the required 99.9% purity required to perform the Sb activation. Thus, the first set of experiments were carried out using high purity Potassium Azide.

Based on the initial promising results, illustrated in the next section of this report, and due to the lack of availability of Cesium Azide we designed and realized an upgraded version of the vacuum setup to experiment the activation of Sb with alkali vapors in a geometrical configuration without line of sight. The new system comprises two vacuum chambers and allowed us to grow cathodes on 100 mm transparent substrates.

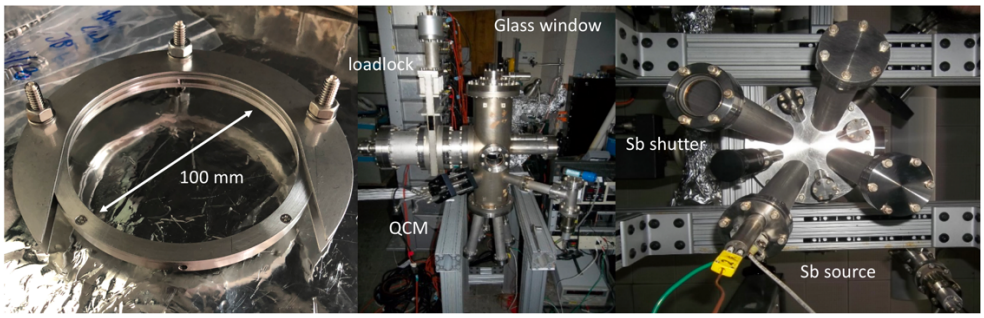

Figure 7. Details of the Sb film growth for 100 mm substrates. Left: the glass holder held into the substrate support structure; Center: the Sb vacuum chamber; Right: a view from the bottom flange hosting the Sb source.

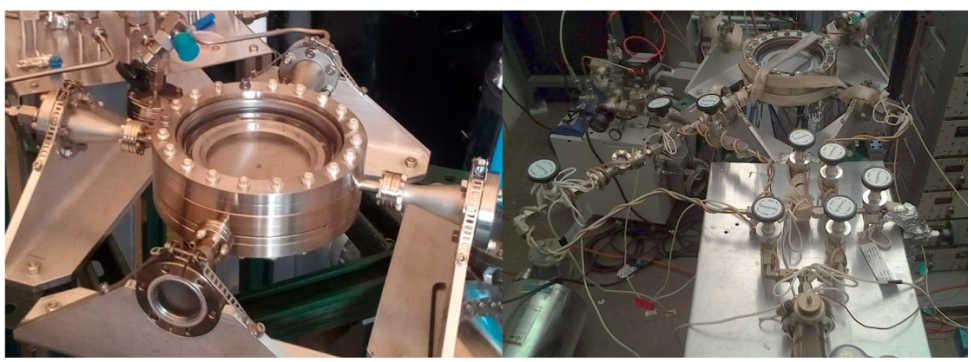

Figure 8. Left: the reaction chamber showing the top glass window and the holder designed to host 100 mm diameter substrates. Right: The reaction chamber connected with the manifold and valve system designed to deliver the alkali metal vapors.

The first chamber (Fig. 7) is used to grow Sb film on a glass or quartz substrate with 100 mm diameter. The Sb growth chamber has been equipped with a load lock chamber that allows loading a new sample without breaking the vacuum of the main chamber who stays insulated by means of a gate valve. After a new sample is loaded the load lock is pumped down using a turbo pump and once vacuum is level is compatible with the growth chamber the gate valve is opened and the holder with glass is inserted into the growth chamber. Here an effusion cells loaded with high purity Sb is used to growth film with thickness measured at the same by a calibrated quartz crystal microbalance and optical thickness (this last is measured at 650 nm using the light of a small laser diode propagating across the vacuum chamber and intercepting the film during the growth). The Sb flux is triggered on and off using a mechanical shutter located in front of the Sb source.

Once the glass sample has been coated with the Sb film it can be extracted to open air amd moved into the reaction chamber shown in Fig. 8. The reaction chamber is designed to mimic the

geometrical constrain encountered into a LAPPD™ or similar device. The inside volume of the reaction chamber has about 150 mm diameter and 20 mm height.

The alkali vapors can be delivered to the reaction chamber using a relatively simple system of tubing. A schematic of the manifold system is provided in Fig. 9.

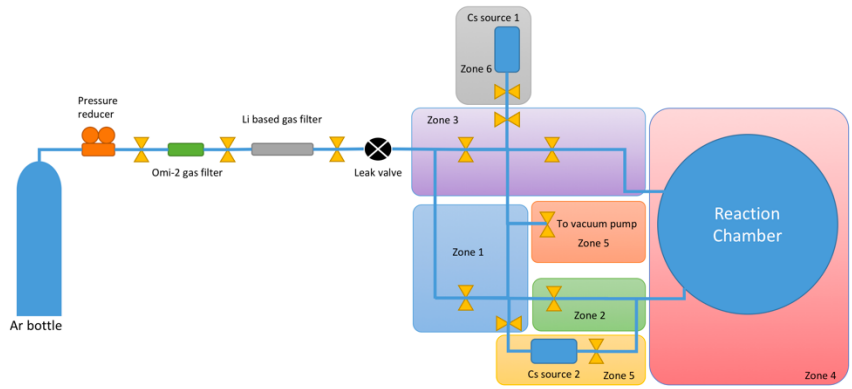

Figure 9. Schematics of the manifold system designed to deliver alkali metal vapors into the reaction chamber hosting the 100 mm diameter samples. The different zones indicated can be set to different temperatures allowing the formation of thermal gradient that induced the diffusion of alkali vapors. On addition high purity Ar gas can be used to facilitate vapor diffusion into the reaction chamber.

4. Photocathode growth using effusion cells

a. Substrates preparation

Photocathode growth experiments were performed on polished 304 stainless steel substrates and on Borofloat 33 glass. The stainless steel substrates were optically polished by using colloidal diamond suspensions with decreasing particulate sizes (from 15 lm to 100 nm). Figure 10 reports a typical surface morphology of the stainless steel substrate after the polishing as obtained using an optical interferometric profiler (ADE Phase Shift MicroXAM). The RMS roughness is determined to be about 3 nm.

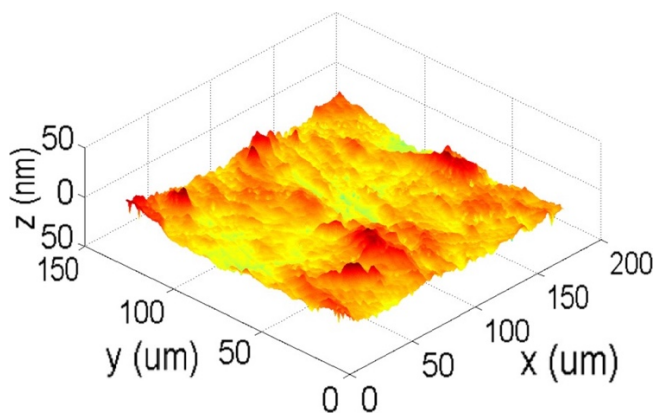

Figure 10. Typical surface morphology of polished stainless steel photocathode substrates.

The 2.5 mm thick Borofloat 33 glass substrates were simply rinsed in isopropyl alcohol then loaded into a dedicated hollow substrate holder, which allows illuminating the photocathode in transmission mode through the back of the substrate. The electrical contact between the photocathode film and the substrate holder is ensured by a 30-micron thick indium metal foil, which is used to solder the retaining mask with the surface of the glass substrate, as shown in Fig. 11.

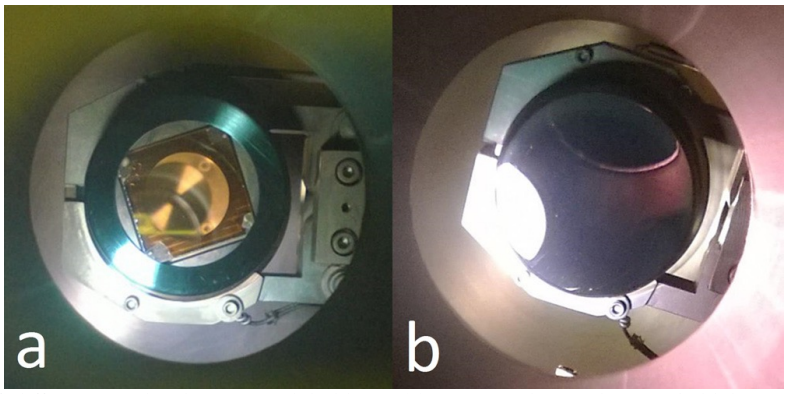

Figure 11. Pictures of different used substrate and holders: (a) square glass substrate held by a metallic retaining ring. Photocathode film is semitransparent. (b) Photocathodes are grown over the polished surface of stainless steel holder. Substrate mirror-like finish is preserved after the growth.

b. Growth using effusion cells

Once substrates have been loaded into the growth chamber, the heater is inserted into the back of the holder (as shown in Fig. 2) and turned on to raise the substrate temperature to 550 °C. During heating, puck and substrate are allowed to degas for at least 24 h until the vacuum pressure in the chamber recovers back to few nTorr. At this point, the substrate temperature is lowered to about 160 °C by decreasing the current through the resistive heater.

c. Sodium Potassium Antimonide growth

A typical growth of a Na_2KSb photocathode proceeds as follows (see Fig. 12). The Sb effusion cell temperature is raised to about 490 °C and a 20nm thin layer of Sb is then deposited over the substrate surface with a quartz microbalance detected deposition rate of about 0.6 nm/min (Sb flux is $4x10^{13}$ atoms $cm^{-2}s^{-1}$).

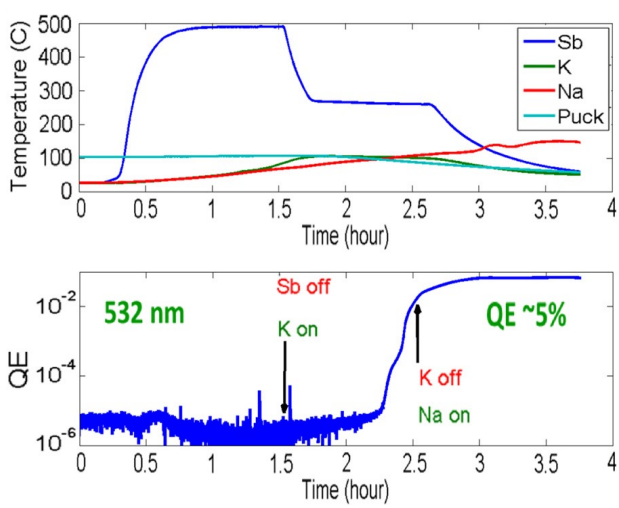

Figure 12. Na_2KSb growth history. Note that according to previous calibrations, the real substrate temperature is about a factor 1.6 larger than the temperature measured at the thermocouple location and here reported.

During the Sb deposition, the temperature of the effusion cell hosting the K is raised to 110 °C. When the growth of the Sb layer is completed, the Sb effusion cell shutter is closed, the temperature of the cell is decreased to 275 °C (preventing alkali metal deposition onto the Sb effusion cell surfaces), and the shutter of the K effusion cell is opened to allow exposure of Sb layer to K vapors (K flux is $3x10^{14}$ atoms $cm^{-2}s^{-1}$). At the same time, the substrate heater is turned

off allowing the substrate to slowly cool down to room temperature by radiative losses. The photocurrent generated by illuminating with a laser light at 532 nm increases as K evaporation continues and is seen to peak when QE reaches about 1%. As the last step, the K effusion cell shutter is closed, and the shutter of the Na effusion cell is opened. The Na effusion cell is heated to 150 °C (Na flux is $3x10^{13}$ atoms $cm^{-2}s^{-1}$), and the photocurrent is seen to further increase up to an equivalent QE of about 5%.

d. Infrared extended sensitive photocathodes

To extend to the IR part of the spectrum, the otherwise limited sensitivity of Na_2KSb photocathodes (to less than 740 nm), we attempted to grow a very thin Cs_3Sb layer over the Na_2KSb. It is expected that due to the formation of a p-n junction at the interface between the intrinsic p-type Na_2KSb and the n-type Cs_3Sb, the photo-excited electrons lying near the bottom of the conduction band within the Na_2KSb layer can travel through the Cs_3Sb and be extracted to vacuum as described in Ref. 27. This mechanism has proven to enable photoemission in the infrared part of the spectrum. A correct dosing of Cs and Sb over the surface of the Na_2KSb photocathode results in an extended response of the photocathode in the infrared all the way to about 1000 nm wavelength. To perform this growth, we used alternating evaporations of Sb and Cs over the surface of several Na_2KSb photocathodes, which were first allowed to cool down to room temperature. During the exposure of the Na_2KSb photocathodes to Cs and Sb vapors, the photocurrent was extracted from the photocathode surface while illuminating the front surface with a laser diode emitting at 780 nm. At this wavelength, a typical Na_2KSb grown using the procedure detailed above has a QE below our detectable threshold (low 10^{-5}) as reported in the spectral response curve shown in Fig. 16. During the exposure of the Na_2KSb photocathodes to alternating Sb and Cs vapors, very small fluxes (on the range of few 10^{12} atoms cm^{-2} s^{-1}) have been used allowing a slow growth and hence a fine tuning of the Cs_3Sb thickness to maximize the QE. The photocurrent extracted at 780 nm was then used as a feedback to trigger the fluxes on and off. Three Na_2KSb photocathodes have been exposed to Cs and Sb vapors (Fig.13). The final QEs obtained at 780 nm with this procedure ranged between $3x10^{-5}$ and $5x10^{-4}$. While these numbers are promising and show that we do extend the sensitivity of our photocathodes to the infrared part of the spectrum, the QEs measured at 780 nm so far were still an order of magnitude lower than those obtained in the photomultiplier tubes for similar materials.

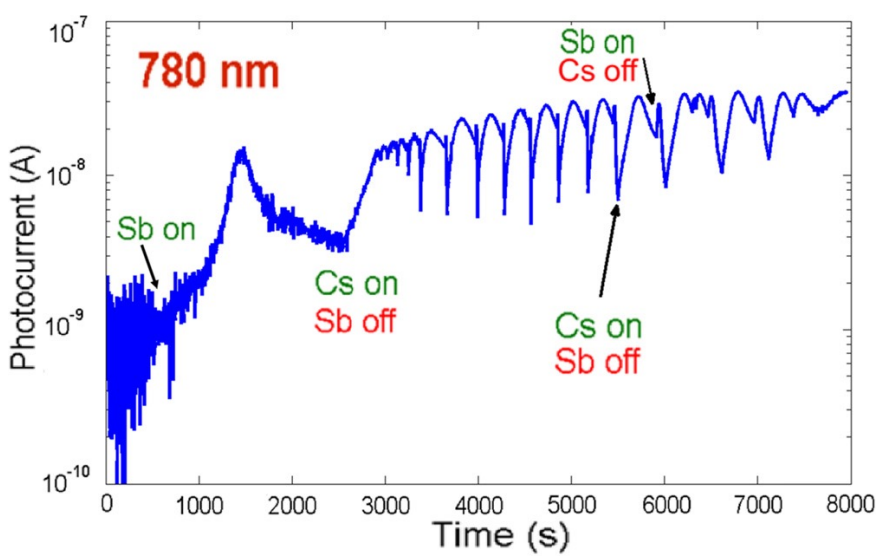

Figure 13. Photocurrent extracted from a Na_2KSb illuminated with light at 780nm during exposure to alternating fluxes of Sb and Cs vapors.

e. Rb based alkali antimonides photocathodes

The growth methods used in the experiments dedicated to the growth of Rb based photocathodes were derived from the recipes previously reported to synthesize other bi-alkali photocathodes based on the sequential evaporation of pure Sb and alkali metals over a suitable substrate (either stainless steel or Borofloat 33 glass).

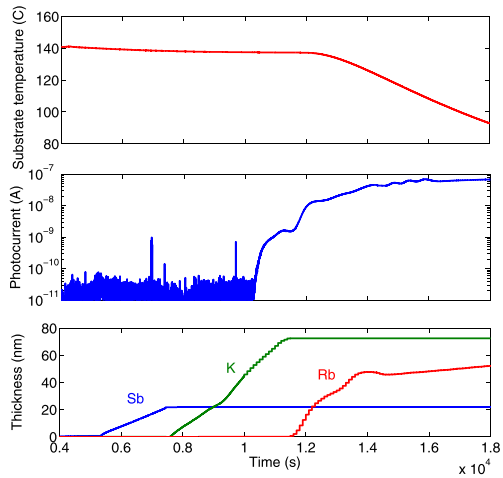

Figure 14. Substrate temperature, photocurrent, and elemental film thickness as measured from Quartz Crystal Microbalance frequency shift during one of the Rb-K-Sb photocathode growth experiments.

The photocurrent produced from the negatively biased thin film under illumination with light at 532 nm is continuously measured during the synthesis procedure. Initial growth of either 10 or 20 nm Sb base layer and exposure of it to K vapors were performed with a roughly constant substrate temperature of about 140 °C. The cooling down to room temperature of the substrate, obtained only by radiative losses, was initiated only once photocurrent first peaked (see Fig. 14) and during exposure to Rb vapors by turning off the substrate heater.

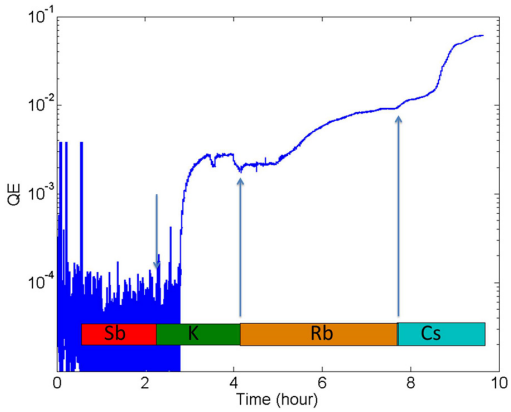

Figure 15. QE as measured during the growth of a semitransparent Cs-Rb-K-Sb photocathode over a Borofloat 33 substrate.

The growth of the Cs-Rb-K-Sb photocathode similarly follows the Rb-K-Sb procedure and is completed with exposure of the photocathode to Cs vapors once the photocurrent extracted during Rb exposure no longer increased, as reported in Fig. 15.

f. Quantum efficiency measurements

The spectral response of one of our Cs-Rb-K-Sb photocathodes is reported in Fig. 16 along with the curves obtained for other cathodes of the alkali antimonide family grown in our laboratory. The spectral response obtained from this multi-alkali antimonide photocathode shows a clear advantage in terms of QE with respect to other bi-alkali photocathodes. At 400nm (the shortest wavelength we can operate which is imposed by limitation of our optical setup), we measured QE of about 25% thus comparable with other high efficiency bi- alkali antimonide photocathodes. On the other hand, in the spectral region between 650 and 750 nm, where most of our bi-alkali antimonides show their photoemission threshold, the efficiency of the multi-alkali Cs-Rb-K-Sb is more than a factor 10 larger than that of our conventional bi-alkali antimonides. The spectral response in the case of Cs-Rb-K-Sb photocathodes extends further towards the infrared part of the spectrum (as compared to other bi-alkali cathodes) up to roughly 800 nm, but for wavelengths longer than 750 nm the Na_2KSb:Cs photocathode still shows the largest sensitivities.

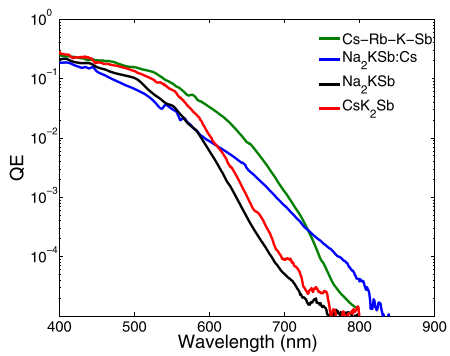

Figure 16. Spectral response of a multi-alkali Cs-Rb-K-Sb photocathode is compared with typical spectral responses of other alkali antimonides grown in our laboratory.

Fig. 17 shows a QE map measured by scanning a focused laser beam (100 microns laser spot diameter) at 532nm over a relatively large area of about 2.2 x 2.2 cm^2 (this area of measurement being limited by the actual measurement setup and substrate size). The resulting map has an average QE of 4.1% with a standard deviation of about 0.2%.

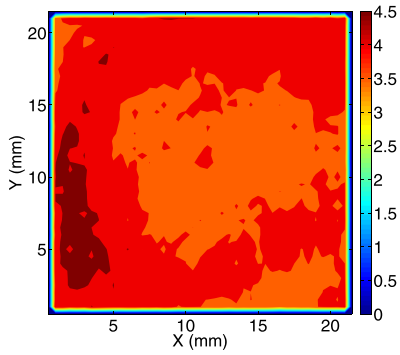

Figure 17. QE map measured by scanning a focused laser beam at 532 nm over a 2.2×2.2 cm2 area of a Rb-K-Sb photocathode: The resulting map has an average QE of 4.1% with a standard deviation of about 0.2%.

For operation in transmission mode (see Fig. 18), which is the mode of operation of photocathodes in many PMTs and LAPPD™ modules, the thickness of the photosensitive material plays also a critical role: if the photocathode material thickness is too large, the excited electrons generated near the interface with the glass have to travel long distances before reaching

the vacuum interface and the increased probability of relaxation and recombination can reduce the effective QE. If the same cathode is operated in reflection mode, such thickness effect is negligible, and QE is not affected by the material to be too thick.

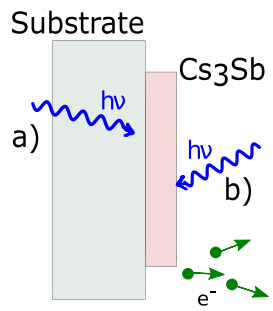

Figure 18. Schematic of the photoemission modes: (a) back-illumination ("transmission mode") and (b) front-illumination ("reflection mode").

QE in transmission and reflection mode of operation was measured for a Rb-K-Sb cathode grown over a glass substrate and reported in Fig. 19. The results indicated a non-efficient operation in transmission mode for wavelengths shorter than 500 nm. On the other hand, a 20% QE was measured at 400 nm in reflection mode. These results indicate that it is likely that the total thickness of the photocathode is too large for optimal operation in transmission mode.

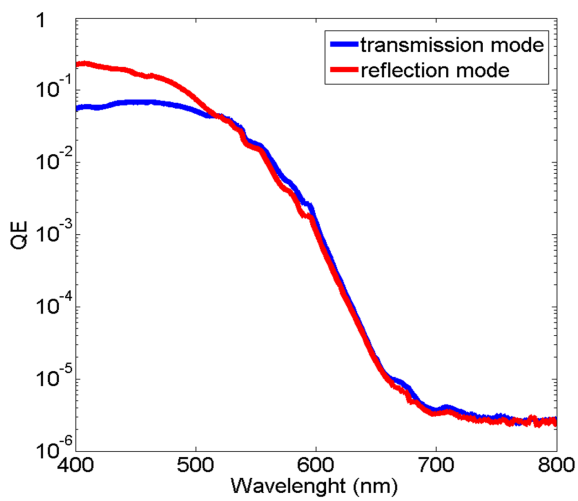

Figure 19. Spectral response of the Rb-K-Sb phtocathode grown over a glass substrates measured for operation in reflection and transmission mode.

5. Photocathode growth using the "in situ" method

A critical step in the fabrication of LAPPD's via the PMT-like in-situ process consists of demonstrating chemical reaction between an Sb layer deposited on glass under vacuum and alkali metal vapors to synthesize the photosensitive material after the Sb has been exposed to ambient air or controlled atmosphere in order to perform the full tile assembly and sealing to incorporate the MCPs and strip line collectors. Fundamental differences between the all-UHV and PMT-like process are illustrated in Fig. 20.

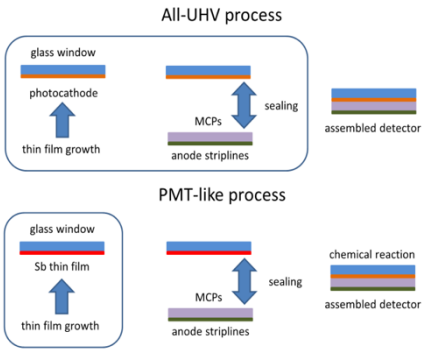

Figure 20. Schematics of the two possible approaches to synthesize and include the photocathode in a planar photodetector.

We performed Cs_3Sb growth experiment to see if the PMT-like path is viable. To this purpose we needed to verify that Sb can react with Cs and yield a photosensitive material after exposure to air or open air. Two Sb film have been grown onto a Si substrate. They were then removed from our growth chamber and moved one at the time into the load lock. The load lock was vented with dry nitrogen. One of the samples was then extracted from the load lock and held in open air for two hours, the other was left into the load lock for the same amount of time and was only exposed to dry nitrogen. After the two hours both samples were moved back into the growth chamber where they were heated to about 130 °C and exposed to Cs vapors from the effusion cell. Both samples were successfully converted into a cesium antimonide photocathode. The spectral responses of these two samples are reported in Fig. 21.

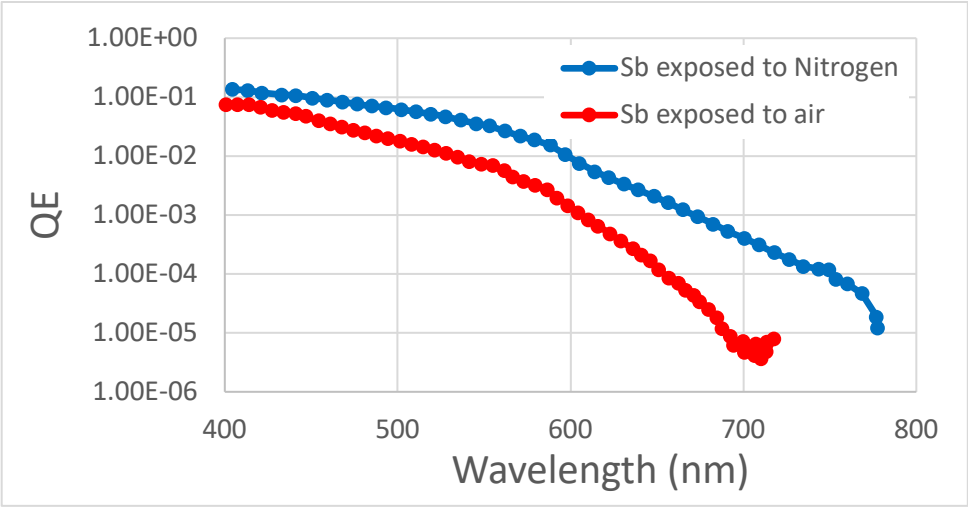

Figure 21. Spectral response of Cs_3Sb obtained with Sb film that have been exposed to either pure nitrogen or air at atmospheric pressure for 2 hours before exposure to Cs vapors.

The results of spectral response seem to indicate that if Sb samples are handled in in dry nitrogen atmosphere photocathodes can be synthesized and QE should reach values similar to the ones obtained in an all-UHV process. If samples are exposed to air it likely that some oxidation of the Sb surface will prevent the photocathode to reach the highest QE but still efficiency on the range a several percent should be reached at the shortest wavelength in the visible region of the spectrum.

Based on these exciting results we grew Sb films onto glass in our effusion cell equipped UHV growth chamber. These films were then extracted from the growth chamber, exposed to air and moved into the reaction chamber shown in Fig. 6. The effusion cell of the reaction chamber was filled with potassium azide. Upon heating of the crucible to about 300 °C the potassium azide decomposed and K vapor migrated into the reaction chamber. We clearly observed (see Fig. 22) the Sb film reacting with potassium vapors and becoming photosensitive (see Fig. 23).

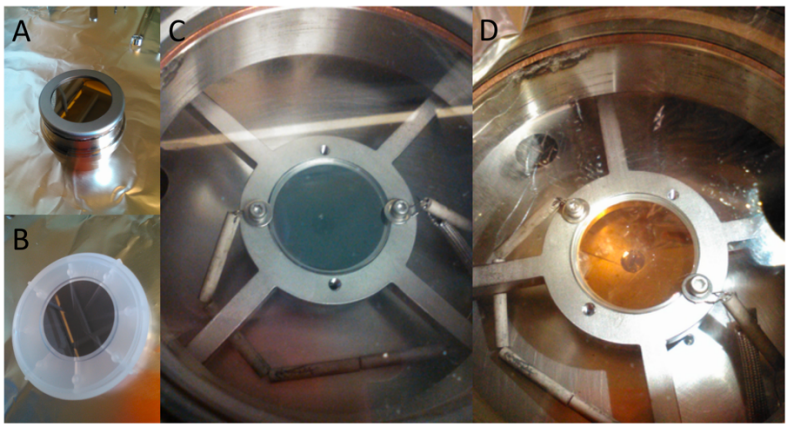

Figure 22. A) The glass substrate mounted onto our sample holde as removed from the load lock after the growth of the Sb film. B) The Sb film on glass substrate removed from the holder ready to be loaded into the reaction chamber. C) the Sb film in the reaction chamber holder before the reaction with alkali metal vapors. D) The Sb film has reacted with alkali metal vapors it has now formed a photosensitive material.

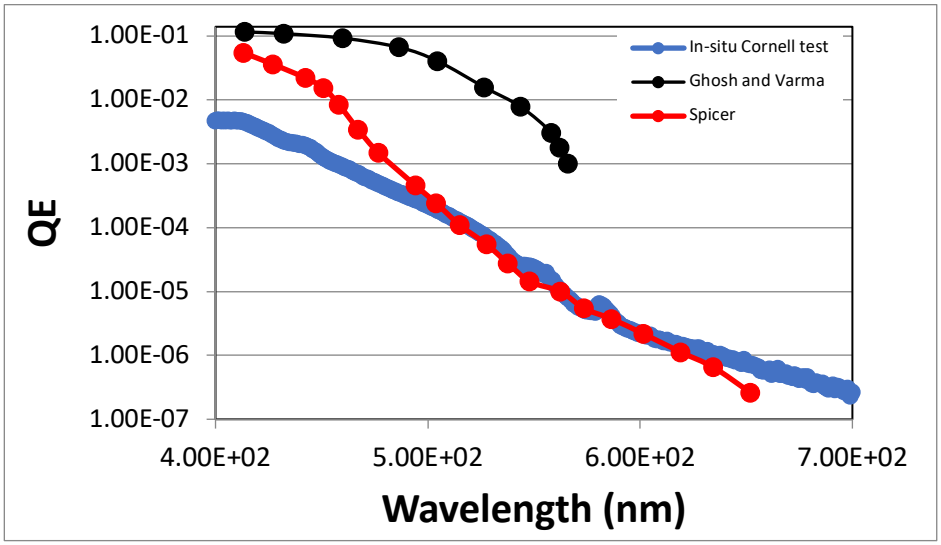

Figure 23. Spectral response of K3Sb synthesized using our in-situ setup compared with data from literature.

Given the lack of availability of high purity cesium azide on the market we decided to develop a manifold to deliver Cs vapors to the reaction chamber using temperature gradient and with the possibility of using Ar gas as carrier. The system was described in Section 3.

Fig. 24 shows a 100 mm fused silica substrate coated with a semitransparent layer of Sb that has been removed frim the load lock of the Sb growth chamber and loaded into the reaction chamber to be exposed to cesium vapors. In order to prevent charge accumulation at the surface a carbon stripe is painted using colloidal carbon across the surface of the substrate.

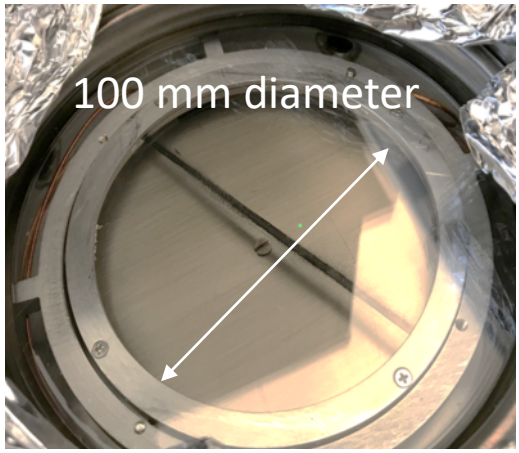

Figure 24. A 100 mm fused silica glass is coated with a semitransparent thin film of Sb and inserted into the reaction chamber. The black stripe is made using UHV colloidal carbon to prevent charge accumulation at the sample surface.

With reference to Fig. 9, the exposure to Cs vapors is triggered by increasing the temperature of the Cs source up to 200 degrees C (zone 5) while the tubulation (zone 2) is held at about 175 degrees C and the whole reaction chamber to about 100 degrees C (zone 4). Photocurrent is measured by collecting the current collected by a plate placed in front of the photocathode with a laser source illuminating the photocathode from the outside trough the UVH window.

During the exposure to Cs vapors the photocurrent is measured and is typically seen to increase and reaching a peak an eventually reach a stable level as seen in Fig. 25.

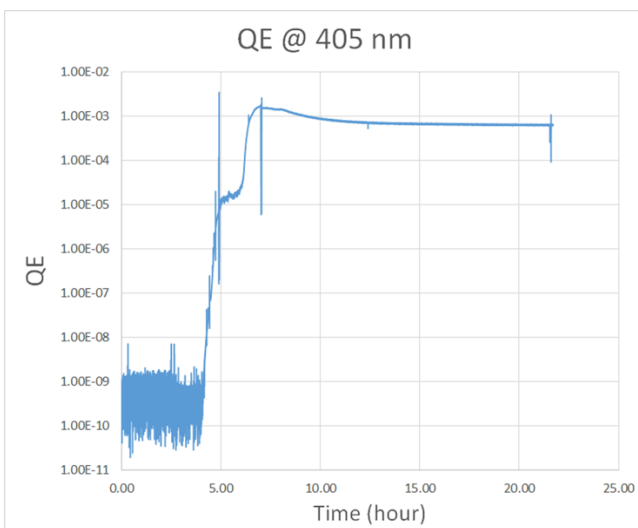

Figure 25. Photocurrent measured on a Cs3Sb during the activation in the reaction chamber.

During and after the exposure to Cs vapors the photocathode is also seen to assume the characteristic yellow-orange coloration. Fig. 26 shows a picture of one of our large area after the reaction with Cs vapor has happened and the correspondent quantum efficiency map measured at 405 nm.

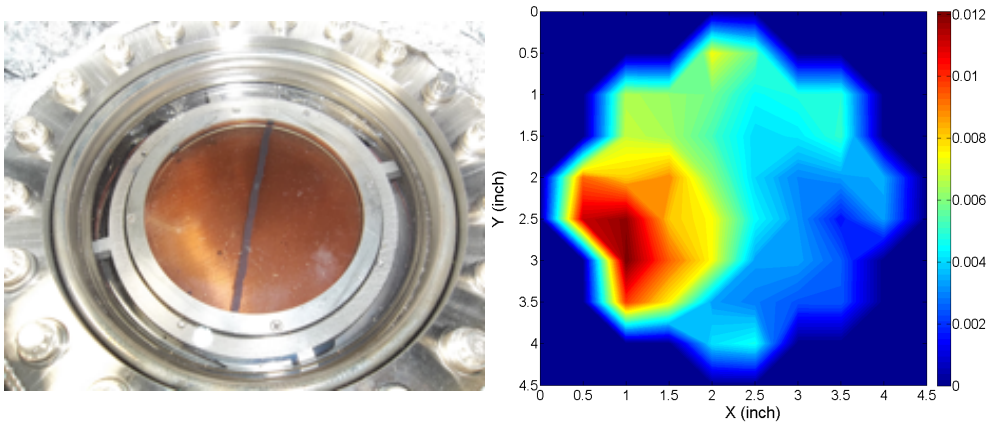

Figure 26. Left: a large area Cs3Sb after the synthesis in the reaction chamber. Right: the correspondent QE map measured at 405 nm.

The largest QE we have achieved (slightly more than 1% at 405 nm) was achieved with an Sb film having about 75% to red light at 650 nm. While these experiment have proven that this could be using the "is-situ" configuration can yield photoemissive materials the phase space of experimental parameter was not sufficiently explored to conclude that this method can yield cathodes with the high QE and uniformity level we achieved using "line of sight" growth experiments.

The vacuum level that is typically in measured in few 10^{-7} Torr might not be sufficiently good for growing alkali antimonides, hence one of the possible improvement consist in the installation of a pump inside the volume of the reaction chamber, which is similar to what is done for PMTs and LAPPD™ modules. Also the non-uniformity of QE seems to be induced by the propagation of the Cs vapors inside the volume hence a dedicated set of experiment that make use of inert carrier gas aimed at improving the diffusion of Cs vapors should be carried out to identify if this is a possible way to address this issue.

Conclusions

We have presented our accomplishments made possible within the DOE award DE-SC0011643 to develop photocathodes for large area photon detector more details can be found in following publications (acknowledging the DOE DE-SC0011643 funding):

- L. Cultrera, J. Bae, I.V. Bazarov, C.J.R. Duncan, A. Galdi, F. Ikponmwen, W. H. Li, J.M. Maxson, C. M. Pierce, "Photocathodes Research Activities for High Brigtheness Beams, Spin Polarized Sources and Large Area Photon Detectors at Cornell University", Proceedings of the 9th International Particle Accelerator Conference, Melbourne, Australia (2017) talk WEXXPLM3
- L. Cultrera, A. Bartnik, I.V. Bazarov, C. Gulliford, P. Gupta, H. Lee, S.A. McBride, T.P. Moore, "Cornell Laboratory for high intensity, ultra-bright and polarized electron beams",

Proceedings of the 8th International Particle Accelerator Conference, Copenhagen, Denmark (2017) paper MOPIK023

- L. Cultera, C. Gulliford, A. Bartnik, H. Lee, I. Bazarov, "Rb based alkali antimonide high quantum efficiency photocathodes for bright electron beam sources and photon detection applications", Journal of Applied Physics 121 (2017) 055306
- P. Gupta, L. Cultrera, I. Bazarov, "Monte Carlo simulations of electron photoemission from cesium antimonide", Journal of Applied Physics 121 (2017) 215702
- L. Cultrera, H. Lee, I.V. Bazarov, "Alkali antimonides photocathodes growth using pure metals evaporation from effusion cells", Journal of Vacuum Science and Technology B 34 (2016) 011202
- H. Lee, L. Cultrera, I.V. Bazarov, "Intrinsic emittance reduction in transmission mode photocathodes", Applied Physics Letters 108 (2016) 124105
- L. Cultrera, C. Gulliford, A. Bartnik, H. Lee, I. Bazarov, "Ultra low emittance electron beams from multi-alkali antimonides photocathodes operated with infrared light", Applied Physics Letters 108 (2016) 134105
- H. Lee, I.V. Bazarov, L. Cultrera, "Intrinsic Emittance Reduction in Transmission Mode Photocathodes", Proceedings of the 6th International Particle Accelerator Conference, Busan, Korea (2016) paper THPOW023 (link).
- L. Cultrera, A.C. Bartnik, I.V. Bazarov, B.M. Dunham, C.M. Gulliford, H. Lee, R.A. Lipton, T.P. Moore, "Photocathode Growth and Characterization Advances at Cornell University", Proceedings of the 6th International Particle Accelerator Conference, Busan, Korea (2016) paper THPOW025

Summary

Alkali antimonide photocathodes can be grown using high purity element evaporated from effusion cell in a line-of-sight geometry which is typical of molecular beam reactors. The photoemission characteristics are directly comparable with the one achieved in PMTs.

The “in-situ” process can in principle a viable option to simplify the manufacturing of LAPPD™ modules and hence lower the cost of production. The initial results indicate indeed that activation of Sb with Cs vapors in a non-line-of-sight configuration is possible. The parameters space needs to be further explored to conclude if this process can yield photoemission properties similar to the previous method.

References

[1] M. Demarteau et al., “Instrumentation Frontier Report”, 2013 “Snowmass” Community Summer Study, in preparation. http://www.snowmass2013.org/tiki-index.php

[2] P. Le Du, “Applications Outside HEP”, Physics Procedia 37 (2012) 34.

[3] LAPPD proposal, June 9, 2009, submitted to the DOE. See http://psec.uchicago.edu/library/

[4] http://hep.uchicago.edu/~frisch/talks/3Yrs_of_LAPPD_Dec_2012_v15.pdf

[5] The University of Chicago has trademarked the 20-cm-square MCP photodetector as LAPPD™, and has licensed the trademark to Incom.

[6] B. Adams, M. Chollet, A. Elagin, Vostrikov, M. Wetstein, R. Obaid, and P. Webster, “A Test-facility for Large-Area Microchannel Plate Detector Assemblies using a Pulse Sub-picosecond Laser”, Rev. Sci. Instrum. 84 (2013) 061301.

[7] B.W. Adams, A. Elagin, H. Frisch, R. Obaid, E. Oberla, A. Vostrikov, R. Wagner, J. Wang, M. Wetstein, “Timing Characteristics of Large Area Picosecond Photodetectors”, Nucl. Instrum. Methods Phys. Res. A 795 (2015) 1.
[8] B. W. Adams, A. Elagin, J. W. Elam, H. J. Frisch, J.-F. Genat, J. S. Gregar, A. U. Mane, M. J. Minot, R. Northrop, R. Obaid, E. Oberla, A. Vostrikov, M. Wetstein, “An Internal ALD-Based High Voltage Divider and Signal Circuit for MCP-based Photodetectors”, Nucl. Instrum. Methods Phys. Res. A 780 (2015) 107.
[9] B. Adams, A. Elagin, H. J Frisch, R. Obaid, E. Oberla, A. Vostrikov, R. G. Wagner and M. Wetstein, “Measurements of the Gain, Time Resolution, and Spatial Resolution of a 20x20cm MCP-based Picosecond Photo-Detector”, Nucl. Instrum. Methods Phys. Res. A 732 (2013) 392.
[10] H. Grabas, R. Obaid, E. Oberla, H. Frisch J.-F. Genat, R. Northrop, F. Tang, D. McGinnis, B. Adams, and M. Wetstein, “RF Strip-line Anodes for Psec Large-area MCP-based Photodetectors”, Nucl. Instrum. Methods Phys. Res. A 711 (2013) 124.
[11] E. Oberla, J.-F. Genat, H. Grabas, H. Frisch, K. Nishimura, and G Varner, “A 15 GSa/s, 1.5 GHz Bandwidth Waveform Digitizing ASIC”, Nucl. Instrum. Methods Phys. Res. A 735 (2014) 452.
[12] M.J. Minot, D. C. Bennis, J.L. Bond, C.A. Craven, A. O′Mahony, J.M. Renaud, M.E. Stochaj, J.W. Elam, A.U. Mane, M.W. Demarteau, R.G. Wagner, J.B. McPhate, O.H. Siegmund, A. Elagin, H.J. Frisch, R.Northrop, M.J. Wetstein, “Pilot production & commercialization of LAPPD™”, Nucl. Instrum. Methods Phys. Res. A 787 (2015) 78.
[13] Steven D. Biller, "Probing Majorana neutrinos in the regime of the normal mass hierarchy." *Physical Review D* 87 (2013) 071301.
[14] C. Aberle, et al. "Measuring Directionality in Double-Beta Decay and Neutrino Interactions with Kiloton-Scale Scintillation Detectors." *arXiv preprint* arXiv:1307.5813 (2013).
[15] “Alkali metals dispensers,” https://www.saesgetters.com/products/alkali- metals-dispensers.
[16] J. Sangster and A. D. Pelton, J. Phase Equilib. 12, 451 (1991).
[17] J. Sangster and A. D. Pelton, J. Phase Equilib. 12, 443 (1991).
[18] A. Petric and A. D. Pelton, J. Phase Equilib. 12, 29 (1991).
[19] F. Blatter and E. Schumacher, J. Less–Common Met. 115, 307 (1986).
[20] L. Cultrera, M. Brown, S. Karkare, W. Schaff, I. Bazarov, and B. Dunham, J. Vac. Sci. Technol. 32, 031211 (2014).
[21] M. A. Mamun, C. Hernandez-Garcia, M. Poelker, and A. A. Elmustafa, APL Mater. 3, 066103 (2015).
[22] N. Massegu, A. Konrath, J. M. Barois, P. Christol, and E. Tourni, Electron. Lett. 44, 315 (2008).
[23] I. A. Dubovoi, A. S. Chernikov, A. M. Prokhorov, M. Y. Schelev, and V. K. Ushakov, Proc. SPIE 1358, 134 (1991).
[24] V. V. Balanyuk, A. S. Chernikov, V. F. Krasnov, S. L. Musher, V. E. Ryabchenko, A. M. Prokhorov, I. A. Dubovoi, V. K. Ushakov, and M. Y. Schelev, Proc. SPIE 945, 68 (1988).
[25] J. Maxson, I. Bazarov, B. Dunham, J. Dobbins, X. Liu, and K. Smolenski, Rev. Sci. Instrum. 85, 093306 (2014).
[26] B. Dunham et al., Appl. Phys. Lett. 102, 034105 (2013).
[27] A. Natarajan, A. T. Kalghatgi, B. M. Bhat, and M. Satyam, J. Appl. Phys. 90, 6434 (2001)